

New materials for optical cooling

S.R. Bowman¹, C.E. Mungan²

¹ Photonics Technology Branch, Naval Research Laboratory, Washington, DC 20375-5320, USA
 (E-mail: bowman@ccf.nrl.navy.mil)

² Department of Physics, U.S. Naval Academy, Annapolis, MD 21402, USA

© Springer-Verlag 2000

Abstract. Well-characterized solid-state laser materials are evaluated for performance in optical refrigeration as well as radiation-balanced laser systems. New figures-of-merit are developed and applied to ytterbium-doped materials. Superior performance is predicted for high-cross-section tungstate materials. Photothermal deflection experiments on samples of Yb³⁺-doped KGd(WO₄)₂ confirm anti-Stokes fluorescence cooling. This is the first observation of optical cooling in a crystal.

PACS: 42.55.Rz; 42.70.Hj

The physical mechanism of radiation cooling by anti-Stokes fluorescence was originally proposed in 1929 [1]. It can be easily understood. Absorption of a photon can, on average, temporarily push an atom away from thermal equilibrium with its surroundings. If the atom then spontaneously emits after thermal equilibrium has been re-established, any frequency shift in the fluorescence compared to the absorbed radiation results in a net heating or cooling of the material. While simple in concept, to obtain radiative cooling in practice requires materials with near-unity fluorescence quantum efficiencies. Such anti-Stokes cooling was first reported in 1981 for CO₂ gas [2], in 1995 and 1996 for organic dye solutions [3, 4], and in 1995 for ytterbium-doped ZBLANP glass [5]. Mungan and Gosnell have published a detailed review of anti-Stokes cooling [6].

Recent commercial availability of high-brightness laser diodes opens the possibility of practical devices that utilize optical cooling. Refinements of the experiments in ytterbium-doped ZBLANP glass have recently demonstrated optical refrigeration from 301 K down to 236 K [7] and modeling suggests that temperatures as low as 77 K can be obtained with this material [8]. Further, it has been proposed that solid-state lasers could be constructed in which the cooling of anti-Stokes fluorescence would offset heat generated by stimulated emission [9]. This mode of laser operation is referred to as radiation-balanced (RB) lasing. Unlike conventional exothermic laser systems, RB lasers would exhibit little or no

internal heat generation. In principle, this technique would allow RB lasers to be scaled up to much higher average powers than conventional solid-state laser systems.

Previous solid-state optical cooling experiments have concentrated on ytterbium-doped glasses [10]. In this paper, we evaluate a range of well-characterized ytterbium-doped laser materials for application to optical refrigeration and radiation-balanced lasing. Crystalline hosts are emphasized instead of glasses because of their generally higher cross sections and well-defined micro-environments. Optical cooling experiments on a few materials confirm the potential of crystals for anti-Stokes optical cooling.

1 Spectral optimization for optical cooling

Detailed descriptions of the process of optical cooling in solids have been presented elsewhere [6–8], so a brief review will suffice here. For ytterbium-doped materials, the process begins with optical pumping near 1.0 μm which excites Yb³⁺ ions from the ²F_{7/2} ground state to the ²F_{5/2} excited state. Both of these states are Stark split into several closely spaced energy levels. The picosecond timescale for phonon coupling of these levels to the lattice combined with the interstate millisecond timescale for spontaneous emission ensures Boltzmann distributions for both of the (2J + 1)/2 multiplets prior to radiative decay. Spontaneous emission of the excited ions yields a broadband fluorescence with a mean wavelength of

$$\lambda_F = \frac{\int I_F(\lambda)\lambda d\lambda}{\int I_F(\lambda)d\lambda}, \quad (1)$$

where $I_F(\lambda)$ is the fluorescence spectral intensity. In the absence of radiative trapping or quenching, a redshift of the pump from the mean wavelength will result in a net cooling of the material. Letting P_F be the total fluorescence power and P_P be the pump power, the efficiency per unit length of the optical cooling process can be defined as

$$\eta_C(\lambda_P) \equiv \frac{1}{P_P} \frac{\partial(P_F - P_P)}{\partial z} = \alpha(\lambda_P) \left(\frac{\lambda_P}{\lambda_F} - 1 \right). \quad (2)$$

Obviously the efficiency initially increases as the pump wavelength, λ_P , is tuned beyond λ_F , but then eventually decreases to zero as the pump absorption coefficient, α falls off. Plotting $\eta_C(\lambda_P)$ will reveal the optimum pump wavelength, λ_{OP} , and best cooling efficiency for a specific temperature and material. As a material figure-of-merit for optical cooling, we will use the more intrinsic quantity

$$F_{\text{cool}} \equiv \frac{\eta_C(\lambda_{OP})}{N_T} = \sigma_A(\lambda_{OP}) \left(\frac{\lambda_{OP}}{\lambda_F} - 1 \right), \quad (3)$$

where N_T is the total active ion density and σ_A is the effective absorption cross section. For a given material, the quantity F_{cool} is readily calculated from measurements of the fluorescence and absorption spectra. Materials with large values of F_{cool} should exhibit high cooling power densities. Note, however, that F_{cool} is only an optical parameter and does not include thermal or mechanical material properties. For instance, in applications where cooling is transferred via conduction, F_{cool} should be divided by the material's thermal conductivity.

2 Spectral optimization for radiation-balanced lasing

Identifying optimal materials for radiation-balanced lasing is a little more involved. As before, the mean fluorescence wavelength, λ_F , is a fixed material parameter given by (1). However, we must choose optimum values of the pump wavelength, λ_P , and the laser wavelength, λ_L , in order to predict a material's RB lasing performance. There are several reasonable parameters on which to perform a comparison of samples. We choose to combine the criteria of optical efficiency and laser gain for optimization. As before, we start by defining an efficiency per unit length for the process,

$$\eta_L(\lambda_P, \lambda_L, I_P) \equiv \frac{1}{I_P} \frac{\partial I_L}{\partial z}, \quad (4)$$

where I_P and I_L are the pump and laser intensities. Using previously derived relations for RB gain [9], (4) can be rewritten as

$$\eta_L(\lambda_P, \lambda_L, I_P) = \frac{\eta_0 \alpha(\lambda_P)}{1 + I_P/I_{P\text{sat}}}. \quad (5)$$

Here η_0 is the RB internal optical efficiency given by

$$\eta_0 = \frac{\lambda_P - \lambda_F}{\lambda_L - \lambda_F}. \quad (6)$$

The RB pump saturation intensity defined in [9] can be written as

$$I_{P\text{sat}} = \frac{hc}{\lambda_F \tau \sigma_A(\lambda_P)} \frac{\lambda_L - \lambda_F}{\lambda_L - \lambda_P} \beta(\lambda_P). \quad (7)$$

Here τ is the spontaneous lifetime of the active ions and $\beta(\lambda)$ is a convenient function involving the effective absorption and emission cross sections:

$$\beta(\lambda) \equiv \frac{\sigma_A(\lambda)}{\sigma_A(\lambda) + \sigma_E(\lambda)}. \quad (8)$$

Similarly, the RB laser saturation intensity defined in [9] can be written as

$$I_{L\text{sat}} = \frac{hc}{\lambda_F \tau \sigma_A(\lambda_L)} \frac{\lambda_P - \lambda_F}{\lambda_L - \lambda_P} \beta(\lambda_L). \quad (9)$$

Unlike simple optical cooling, the RB lasing process requires minimum intensities for both the pump and laser fields. The minimum pump intensity [9] can be written as

$$I_{P\text{min}} = \frac{\beta(\lambda_L)}{\beta(\lambda_P) - \beta(\lambda_L)} I_{P\text{sat}} \quad (10)$$

and the minimum laser intensity [9] as

$$I_{L\text{min}} = \frac{\beta(\lambda_P)}{\beta(\lambda_P) - \beta(\lambda_L)} I_{L\text{sat}}. \quad (11)$$

The efficiency in (5) has its largest value when the pump intensity is minimal, $I_P = I_{P\text{min}}$. Therefore RB lasers will have their highest efficiency when we select conditions to optimize the quantity

$$\frac{\eta_L(\lambda_P, \lambda_L, I_{P\text{min}})}{N_T} = \sigma_A(\lambda_P) \frac{\beta(\lambda_P) - \beta(\lambda_L)}{\beta(\lambda_P)} \frac{\lambda_P - \lambda_F}{\lambda_L - \lambda_F}. \quad (12)$$

Optimizing the efficiency leads to a clear choice for the pump wavelength. However, (12) is only a weak function of the laser wavelength. This residual ambiguity allows us to also optimize the laser gain. The maximum small-signal gain coefficient consistent with RB laser operation, g_{max} , can be written as [9]

$$\frac{g_{\text{max}}}{N_T} = \sigma_A(\lambda_L) \frac{\beta(\lambda_P) - \beta(\lambda_L)}{\beta(\lambda_L)}. \quad (13)$$

This is the gain that occurs with saturated pumping ($I_P \gg I_{P\text{sat}}$) and minimal injected RB laser intensity. In order to optimize both gain and efficiency, we select the laser wavelength, λ_{OL} , and pump wavelength, λ_{OP} , that maximize the product of (12) and (13). This procedure gives unambiguous optimal values for both wavelengths. We can now define figures-of-merit for RB laser materials as

$$F_{\text{eff}} \equiv \sigma_A(\lambda_{OP}) \frac{\beta(\lambda_{OP}) - \beta(\lambda_{OL})}{\beta(\lambda_{OL})} \frac{\lambda_{OP} - \lambda_F}{\lambda_{OL} - \lambda_F} \quad (14)$$

and

$$F_{\text{gain}} \equiv \sigma_A(\lambda_{OL}) \frac{\beta(\lambda_{OP}) - \beta(\lambda_{OL})}{\beta(\lambda_{OL})}. \quad (15)$$

Materials with high values of F_{eff} and F_{gain} should exhibit superior performance as radiation-balanced lasers.

The optimization scheme described above is convenient and robust for a broad range of materials. It gives a good compromise between best efficiency and best gain. In practice however, a laser designer may elect to minimize the required pump intensity in order to facilitate construction of the pump source. Alternatively, one may choose to increase the separation between pump and laser wavelengths to facilitate optical coatings or optimize the laser for best gain. The impact of shifting the operating wavelengths varies substantially from one laser material to another. In the next section we will use (3), (14), and (15) to compare some well-known ytterbium-doped materials.

3 Comparison of ytterbium-doped materials

The figures-of-merit developed in the previous section can be immediately computed for any material and temperature from precise absorption and emission cross-section spectra. However, since these figures-of-merit are quite sensitive to weak absorption in the long-wavelength wings, it is often preferable to use the reciprocity principle for the calculations. If the energy levels of the upper and lower manifolds are known, then the red wing of the absorption cross section can usually be more accurately calculated from the emission data. Also the $\beta(\lambda)$ functions can be computed directly using

$$\beta(\lambda) = \left[1 + \frac{Z_1}{Z_2} \exp\left(\frac{\varepsilon_2}{kT} - \frac{hc}{\lambda kT}\right) \right]^{-1}. \quad (16)$$

Here Z_2 and Z_1 are the thermal partition functions of the upper and lower states, and ε_2 is the energy difference between the lowest levels in these two states.

Eighteen different ytterbium-doped laser materials were evaluated using the figures-of-merit for optical cooling and RB lasing. Emission and absorption spectral data for each material were digitized from previous reports in the literature [6, 11–25]. Reported values of the energy levels within the $^2F_{7/2}$ ground state and the $^2F_{5/2}$ excited state were used to compute the partition and $\beta(\lambda)$ functions. When necessary, emission spectra were scaled to effective cross sections through comparison with the reciprocity-calculated wing emission. The scale of each emission spectrum was checked with the reported fluorescence lifetime via the Fuchtbauer–Ladenburg equation. Where possible, carefully measured laser absorption coefficients were used to check the published spectra. Reported absorption spectra were also compared to measured spectra on the samples tested for optical cooling which are discussed in the next section. For anisotropic materials, polarized emission data were averaged to compute λ_F and the pump and laser polarizations were selected to optimize the figures-of-merit. For a few materials, no reports of the manifold energy levels were found in the literature. In

these cases, the room-temperature partition functions were approximated as unity. Numerical studies on the well-known materials revealed that this approximation only weakly impacts the results of the calculations.

Table 1 lists the properties of the ytterbium materials analyzed in order of decreasing F_{cool} . The cooling figures-of-merit for $\text{KY}(\text{WO}_4)_2$ and $\text{KGd}(\text{WO}_4)_2$ are by far the largest. Other good candidates for optical cooling are $\text{Lu}_3\text{Al}_5\text{O}_{12}$ and $\text{Sr}_5(\text{VO}_4)_3\text{F}$. As expected, the low cross section of ZBLANP glass puts it near the bottom of the list. Again, F_{cool} is based only on room-temperature spectral data and does not include the effects of Yb^{3+} concentration or thermal properties.

The predicted performance for radiation-balanced lasing is graphed in Fig. 1. Note the wide range of values that these materials exhibit. This is because RB lasers are very sensitive to the shape as well as the magnitude of the red-wing spectral data. Broad spectral bands and high cross sections

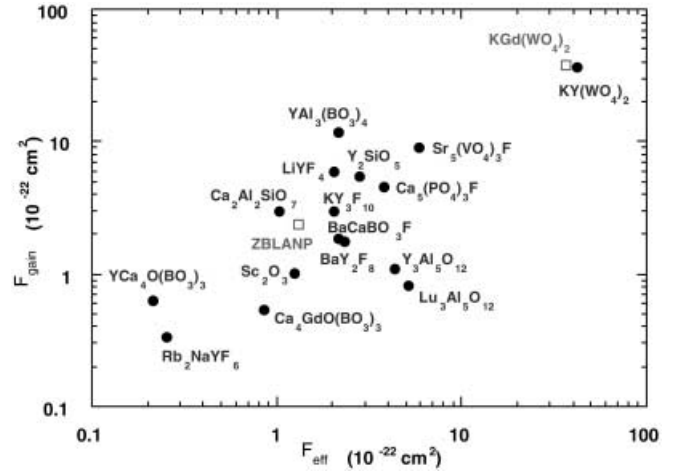


Fig. 1. Figures-of-merit for ytterbium one-micron radiation-balanced lasers. Higher values are preferred. The analysis was performed assuming room-temperature operation. *Open squares* indicate materials for which optical cooling has been demonstrated

Table 1. Parameters characterizing the optical cooling and RB lasing of 18 different Yb^{3+} doped materials. The wavelengths λ_{OP} and λ_{OL} are optimized for RB lasing; the pump wavelength optimizing optical cooling is only slightly different than the former

Host	λ_F nm (polarization)	λ_{OP}	λ_{OL}	η_0 %	τ ms	I_{pmin} kW/cm ²	I_{Lmin}	Z_1/Z_2 at 295 K	F_{cool}	F_{eff} 10 ⁻²² cm ²	F_{gain}	Ref.
$\text{KY}(\text{WO}_4)_2$	992	1002 (a)	1041 (b)	20	0.60	1.6	5.5	1.23	1.50	41	36	11–13
$\text{KGd}(\text{WO}_4)_2$	993	1001 (a)	1042 (b)	17	0.60	1.3	4.3	1.23	1.33	36	37	11–13
$\text{Lu}_3\text{Al}_5\text{O}_{12}$	1002	1033	1048	67	0.92	26	303	0.89	0.49	5.1	0.83	14
$\text{Sr}_5(\text{VO}_4)_3\text{F}$	1041	1047 (π)	1117 (π)	8	0.59	0.14	1.6	1	0.45	5.8	9.2	15–16
$\text{Ca}_5(\text{PO}_4)_3\text{F}$	1033	1046 (π)	1123 (π)	14	1.10	0.14	2.9	1	0.35	3.8	4.6	17
$\text{Y}_3\text{Al}_5\text{O}_{12}$	1007	1031	1049	56	0.95	15	133	0.88	0.32	4.3	1.1	18
BaCaBO_3F	1020	1035 (π)	1084 (σ)	22	1.17	1.7	20	1	0.19	2.1	1.9	19
Y_2SiO_5	1001	1007 (x)	1036 (y)	18	1.04	11	18	1	0.15	2.8	5.5	20
BaY_2F_8	995	1015 (y)	1030 (y)	58	2.04	51	97	1	0.14	2.3	1.8	20
Sc_2O_3	1022	1042	1095	27	0.80	2.3	34	1	0.13	1.25	1.0	22
KY_3F_{10}	992	1003	1014	49	1.87	63	64	1	0.12	2.0	3.0	20
$\text{YAl}_3(\text{BO}_3)_4$	999	1008 (σ)	1037 (σ)	22	0.68	21	13	1.19	0.114	2.1	12	21
LiYF_4	996	1004 (π)	1017 (π)	41	2.21	34	19	0.90	0.108	2.0	6.0	20
$\text{Ca}_2\text{Al}_2\text{SiO}_7$	1012	1028 (σ)	1081 (σ)	22	0.82	4.7	16	1.17	0.077	1.02	3.0	23
ZBLANP	995	1005	1024	36	1.70	38	46	1.07	0.070	1.32	2.4	6
$\text{Ca}_4\text{GdO}(\text{BO}_3)_3$	1011	1032 (z)	1083 (x)	30	2.50	2.5	35	1.18	0.068	0.84	0.54	24
Rb_2NaYF_6	996	1011	1068	20	10.8	1.8	17	1	0.020	0.25	0.34	20
$\text{YCa}_4\text{O}(\text{BO}_3)_3$	1035	1047 (z)	1084 (x)	25	2.28	8.9	15	0.96	0.013	0.21	0.63	25

are very favorable. Based on this spectral analysis, we predict that Yb^{3+} -doped $\text{KY}(\text{WO}_4)_2$ and $\text{KGd}(\text{WO}_4)_2$ will exhibit superior laser performance in RB laser systems. They exhibit figures-of-merit nearly an order of magnitude higher than any other material considered.

These predictions are based on the assumption that the materials can exhibit near-unity quantum efficiency in practice. The validity of this assumption is tested in the next section.

4 Experimental Results

A photothermal deflection spectrometer was constructed using a tunable titanium–sapphire laser as the pump source and a helium–neon laser as the probe, as sketched in Fig. 2. The cw pump source was chopped at a slow rate and focused into a sample material. The helium–neon probe beam counter-propagates through the sample and is slightly deflected by the thermal transient. Deflections are measured several meters away on a large-area dual-cathode silicon diode. With minimum vibrations and air turbulence, angular deflections as small as $0.01 \mu\text{rad}$ could be resolved. The sample materials were fabricated as oriented polished cubes approximately 1 cm on an edge. A small-diameter probe beam ($50 \mu\text{m}$) ensures that the photothermal deflection is not sensitive to radiation trapping inside the uncoated samples. Tuning of the pump source allows for direct determination of the heat generated by the pump absorption. As the pump beam is tuned to longer wavelengths the amplitude of the deflection decreases. Optical cooling is indicated by a change in the sign of the transient deflection. Used in this way, the photothermal deflection technique can detect small deviations from ideal radiative decay.

To test the predictions of the previous section, photothermal deflection experiments were conducted on high-quality samples of lightly ytterbium-doped $\text{Y}_3\text{Al}_5\text{O}_{12}$ (YAG), LiYF_4 (YLF), $\text{KGd}(\text{WO}_4)_2$ (KGW) and ZBLANP. Optical cooling was observed at long wavelengths for the samples of KGW and ZBLANP, whereas only heating was observed for the YAG and YLF samples. Slow chopping of the pump beam produces probe deflection transients similar to those shown in Fig. 3. The pump pulse duration was nominally 50 ms. The

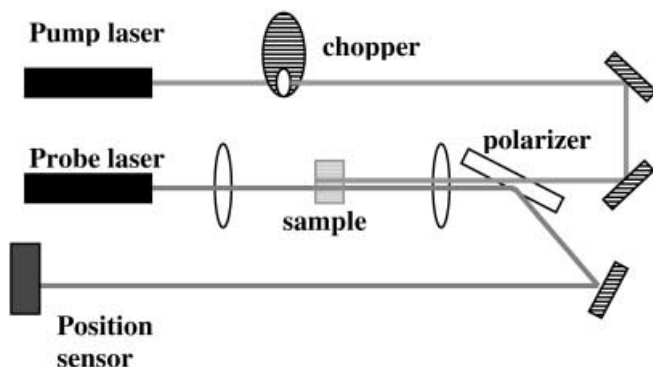


Fig. 2. Pump-probe photothermal deflection experiment. The pump source was a cw titanium–sapphire laser. The probe source was a 632.8-nm helium–neon laser. A polarized beam splitter in combination with narrow bandpass filters rejected pump light and spurious probe reflections from the position sensor

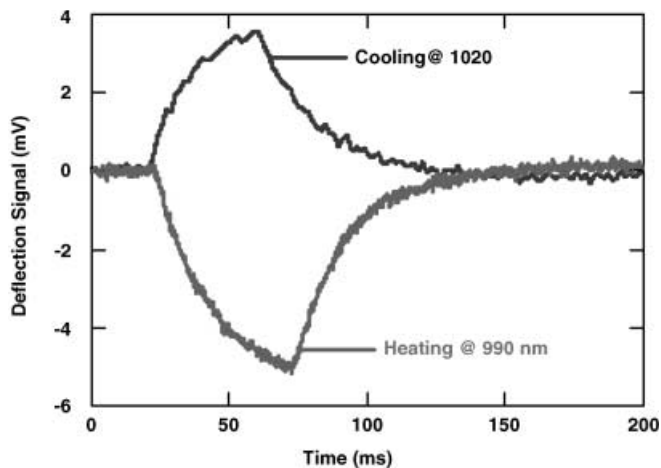


Fig. 3. Typical photothermal deflection transients for 3.5 at. % Yb^{3+} -doped $\text{KGd}(\text{WO}_4)_2$. Optical cooling is inferred when the deflection transient changes sign. For this sample the crossover occurs when the *a*-axis polarized pump beam is tuned to 1008 nm. Similar deflection waveforms and crossover wavelengths were observed for the *b*-axis and *c*-axis polarizations

peak deflection signals were recorded over a tuning range of 940 to 1030 nm. Over this tuning range, the recorded cw incident pump power varied from 1.5 to 0.02 W. Weak green fluorescence at 530 to 560 nm was visible in all samples, indicating some level of residual impurities, possibly erbium.

Analysis of the photothermal deflection signals at different pump wavelengths reveals the radiative efficiency of these samples. Mungan and Gosnell have shown that this type of data can be fit to a simple rate equation model [6]. This model includes steady-state excitation and spontaneous emission of the $\text{Yb}^{3+} \ ^2F_{5/2}$ level. To account for possible heating due to nonradiative decay routes, they included a background non-saturable pump absorption coefficient, α_b , and a direct linear quenching power per ion, κ . According to the model, the spectral dependence of the rate of laser-induced heating, \dot{q} , is given by

$$\frac{\dot{q}}{I_P} = \left(1 - \frac{\lambda_P}{\lambda_F} + \frac{\kappa \lambda_P \tau}{hc} \right) \alpha(\lambda_P) + \alpha_b, \quad (17)$$

where I_P is the pump intensity and $\alpha(\lambda_P)$ is the Yb^{3+} absorption coefficient. Since the photothermal deflection signal, $PTD(\lambda_P)$, is proportional to \dot{q} , this theory predicts a nearly linear wavelength dependence of $PTD(\lambda_P)$ normalized by the absorbed power density,

$$\frac{PTD(\lambda_P)}{\alpha(\lambda_P) I_P} \propto 1 + \left(\frac{\kappa \tau}{hc} - \frac{1}{\lambda_F} \right) \lambda_P + \frac{\alpha_b}{\alpha(\lambda_P)}. \quad (18)$$

Indeed, all of the samples tested exhibited a linear spectral dependence of normalized deflection data, as shown in Fig. 4.

The proportionality constant in (18) depends on precise details of the thermo-optic transport process and the deflection geometry. However, the predicted linearity of the data allows an analysis without knowledge of this constant. Let λ_0 represent the pump wavelength of the photothermal deflection crossover from heating to cooling. The degree of nonradiative decay in a particular sample can then be quantified by the fractional shift in the actual deflection crossover from that of

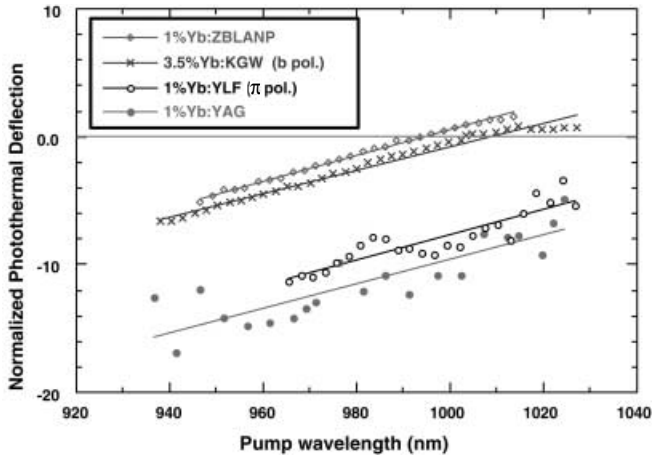


Fig. 4. Normalized deflection signal as a function of pump wavelength. Negative signals indicate heating, and positive signals indicate cooling. The pump polarizations are indicated in parentheses for the anisotropic samples

an ideal radiator,

$$\frac{\lambda_0 - \lambda_F}{\lambda_F} = \frac{\alpha_b}{\alpha(\lambda_0)} + \frac{\kappa\tau\lambda_0}{hc}. \quad (19)$$

In words, this fractional shift in the *PTD* crossover wavelength is simply equal to the fractional radiative deficiency given by the sum of the ratio of the extrinsic to the intrinsic absorption plus the fraction of excited ytterbium ions that decay via quenching.

Using the intercept analysis of (19), the samples of ZBLANP and KGW are found to exhibit 0.0% and 1.6% degrees of nonradiative decay, respectively. Further the deviation for KGW is small enough that it may be caused by inaccuracies in the spectral data of this new material. Fluorescence and absorption data on the other samples are much better known and therefore estimates of the actual mean fluorescence wavelength, λ_F , are more reliable. Since both of these materials exhibit near-unity radiative efficiencies, the figure-of-merit analysis for optical cooling and RB lasing should apply. Extrapolating the deflection crossovers for the YLF and YAG samples in Fig. 4 yields estimates of 8.0% and 9.2% degrees of nonradiative decay, respectively. These are significant heat generation rates even for conventional Yb^{3+} laser systems. Clearly, further work on material refinement will be required to identify this loss mechanism and improve these laser materials.

5 Summary

Crystalline hosts for trivalent ytterbium ions are examined for optical refrigeration and radiation balanced lasing applications. A spectral analysis of many ytterbium-doped materials reveals $\text{KY}(\text{WO}_4)_2$ and $\text{KGd}(\text{WO}_4)_2$ to be the most promising. Because of their high cross sections, these crystals have a figure-of-merit for optical cooling 20 times higher than the previously investigated ZBLANP glass. For radiation-balanced lasing, $\text{KGd}(\text{WO}_4)_2$ has figures-of-merit an order

of magnitude higher than those of $\text{Yb}:\text{YAG}$, the most widely used 1.03- μm laser material. Optical pumping experiments confirm the potential of these tungstate materials. Anti-Stokes cooling is reported at room temperature in 3.5% Yb -doped $\text{KGd}(\text{WO}_4)_2$ crystals. Initial as-obtained samples of this material exhibited a 98.4% radiative efficiency. This is the first report of optical cooling in a crystal and confirms the importance of this class of Yb^{3+} -doped materials for future applications.

Acknowledgements. This work was supported by the Office of Naval Research. We also thank T.R. Gosnell for valuable discussions and for the loan of the ZBLANP sample used in this study.

References

1. P. Pringsheim: *Z. Phys.* **57**, 739 (1929)
2. N. Djeu, W.T. Whitney: *Phys. Rev. Lett.* **46**, 236 (1981)
3. C. Zander, K.H. Drexhage: In *Advances in Photochemistry*, Vol. 20, ed. by D.C. Neckers, D.H. Volman, G. von Büнау (Wiley, New York 1995) pp. 59–78
4. J.L. Clark, G. Rumbles: *Phys. Rev. Lett.* **76**, 2037 (1996)
5. R.I. Epstein, M.I. Buchwald, B.C. Edwards, T.R. Gosnell, C.E. Mungan: *Nature (London)* **377**, 500 (1995)
6. C.E. Mungan, T.R. Gosnell: *Adv. At. Mol. Opt. Phys.* **40**, 161 (1999)
7. T.R. Gosnell: *Opt. Lett.* **24**, 1041 (1999)
8. G. Lamouche, P. Lavallard, R. Suris, R. Grousson: *J. Appl. Phys.* **84**, 509 (1998)
9. S.R. Bowman: *IEEE J. Quantum Electron.* **QE-35**, 115 (1999)
10. G. Lei, J.E. Anderson, M.I. Buchwald, B.C. Edwards, R.I. Epstein, M.T. Murtagh, G.H. Sigel, Jr.: *IEEE J. Quantum Electron.* **QE-34**, 1839 (1998)
11. N.V. Kuleshov, A.A. Lagatsky, V.G. Shcherbitsky, V.P. Mikhailov, E. Heumann, T. Jensen, A. Diening, G. Huber: *Appl. Phys. B* **64**, 409 (1997)
12. N.V. Kuleshov, A.A. Lagatsky, A.V. Podlipensky, V.P. Mikhailov, G. Huber: *Opt. Lett.* **22**, 1317 (1997)
13. Material data sheets on $\text{Yb:KY}(\text{WO}_4)_2$ and $\text{Yb:KGd}(\text{WO}_4)_2$ from Thor Labs Inc.
14. D.S. Sumida, T.Y. Fan, R. Hutcheson: *OSA Proceedings on Advanced Solid-State Lasers Vol. 24*, ed. by B.H.T. Chai, S.A. Payne (Optical Society of America, Washington, D.C. 1995) pp. 384–350
15. L.D. DeLoach, S.A. Payne, W.L. Kway, J.B. Tassano, S.N. Dixit, W.F. Krupke: *J. Lumin.* **62**, 85 (1994)
16. S.A. Payne, L.D. DeLoach, L.K. Smith, W.F. Krupke, B.H.T. Chai, G. Loutts: *OSA Proceedings on Advanced Solid-State Lasers Vol. 20*, ed. by T.Y. Fan, B.H.T. Chai (Optical Society of America, Washington, D.C. 1994) pp. 95–99
17. S.A. Payne, L.K. Smith, L.D. DeLoach, W.L. Kway, J.B. Tassano, W.F. Krupke: *IEEE J. Quantum Electron.* **QE-30**, 170 (1994)
18. H.W. Bruesselbach, D.S. Sumida, R.A. Reeder, R.W. Byren: *IEEE J. Sel. Top. Quantum Electron.* **3**, 105 (1997)
19. K.I. Schaffers, L.D. DeLoach, S.A. Payne: *IEEE J. Quantum Electron.* **QE-32**, 741 (1996)
20. L.D. DeLoach, S.A. Payne, L.L. Chase, L.K. Smith, W.L. Kway, W.F. Krupke: *IEEE J. Quantum Electron.* **QE-29**, 1179 (1993)
21. P. Wang, J.M. Dawes, P. Dekker, D.S. Knowles, J.A. Piper, B. Lu: *J. Opt. Soc. Am. B* **16**, 63 (1999)
22. L. Fornasiero, E. Mix, V. Peters, K. Petermann, G. Huber: *Cryst. Res. Technol.* **34**, 255 (1999)
23. B. Simondi-Teisseire, B. Viana, D. Vivien, A.M. Lejus: *Phys. Status Solidi A* **155**, 249 (1996)
24. F. Mougel, K. Dardenne, G. Aka, A. Kahn-Harari, D. Vivien: *J. Opt. Soc. Am. B.* **16**, 164 (1999)
25. D.A. Hammons, L. Shah, J. Eichenholz, Q. Ye, M. Richardson, B.H.T. Chai, A. Chin, J. Cary: *OSA Proceedings on Advanced Solid-State Lasers, Vol. 26*, ed. by M.M. Fejer, H. Injeyan, U. Keller (Optical Society of America, Washington, D.C. 1999) pp. 286–290